Geophysical Research Letters

RESEARCH LETTER
10.1029/2022GL101750

Atmospheric River Contributions to Ice Sheet Hydroclimate at the Last Glacial Maximum

Christopher B. Skinner[1], Juan M. Lora[2], Clay Tabor[3], and Jiang Zhu[4]

[1]Department of Environmental, Earth and Atmospheric Sciences, University of Massachusetts Lowell, Lowell, MA, USA, [2]Department of Earth and Planetary Sciences, Yale University, New Haven, CT, USA, [3]Department of Geosciences, University of Connecticut, Storrs, CT, USA, [4]Climate and Global Dynamics Laboratory, NCAR, Boulder, CO, USA

Key Points:

- Atmospheric rivers were less frequent and supplied less precipitation globally during the Last Glacial Maximum (LGM)
- Over land, atmospheric river precipitation peaked along the margins of the extratropical ice sheets
- Atmospheric rivers were important contributors to the surface mass balance of LGM ice sheets

Supporting Information:

Supporting Information may be found in the online version of this article.

Correspondence to:

C. B. Skinner,
christopher_skinner@uml.edu

Citation:

Skinner, C. B., Lora, J. M., Tabor, C., & Zhu, J. (2023). Atmospheric river contributions to ice sheet hydroclimate at the Last Glacial Maximum. *Geophysical Research Letters*, *50*, e2022GL101750. https://doi.org/10.1029/2022GL101750

Received 19 OCT 2022
Accepted 23 NOV 2022

Author Contributions:

Conceptualization: Christopher B. Skinner, Juan M. Lora
Formal analysis: Christopher B. Skinner
Funding acquisition: Christopher B. Skinner, Juan M. Lora
Investigation: Juan M. Lora
Methodology: Christopher B. Skinner, Juan M. Lora, Jiang Zhu
Writing – original draft: Christopher B. Skinner, Juan M. Lora, Clay Tabor, Jiang Zhu
Writing – review & editing: Christopher B. Skinner, Juan M. Lora, Clay Tabor, Jiang Zhu

Abstract Atmospheric rivers (ARs) are an important driver of surface mass balance over today's Greenland and Antarctic ice sheets. Using paleoclimate simulations with the Community Earth System Model, we find ARs also had a key influence on the extensive ice sheets of the Last Glacial Maximum (LGM). ARs provide up to 53% of total precipitation along the margins of the eastern Laurentide ice sheet and up to 22%–27% of precipitation along the margins of the Patagonian, western Cordilleran, and western Fennoscandian ice sheets. Despite overall cold conditions at the LGM, surface temperatures during AR events are often above freezing, resulting in more rain than snow along ice sheet margins and conditions that promote surface melt. The results suggest ARs may have had an important role in ice sheet growth and melt during previous glacial periods and may have accelerated ice sheet retreat following the LGM.

Plain Language Summary During the Last Glacial Maximum (~21,000 years ago), ice sheets covered much of northern North America, Fennoscandia, and the Patagonian Andes. Using climate model simulations, we find that much of the precipitation that fell on the margins of these ice sheets came from transient, narrow corridors of atmospheric moisture known as atmospheric rivers. The atmospheric rivers were important in driving ice sheet accumulation during cold seasons, and ice sheet melt during warm seasons. The results suggest that atmospheric rivers may have had a role in driving the movement of ice sheets during Earth's past.

1. Introduction

Atmospheric rivers (ARs) are transient, narrow corridors of concentrated moisture and heat transport (Shields et al., 2019; Zhu & Newell, 1998). They often form near the cold fronts of marine extratropical cyclones where evaporation is high and poleward flow is strong (Dacre et al., 2015; Zhang et al., 2019). Though usually confined to the mid latitudes, ARs occasionally extend toward Earth's poles, making landfall along the Greenland and Antarctic ice sheets (Gorodetskaya et al., 2014; Neff et al., 2014; Wille et al., 2021). Upon landfall, air within the AR is forced upward along the orographic barrier of the ice sheets, resulting in condensation and precipitation. During the winter, spring, and fall seasons, AR precipitation primarily falls as snow, adding more than 10 mm water equivalent per day to surface mass balance (SMB; the difference between accumulation and ablation) in portions of Greenland (Mattingly et al., 2018), and contributing up to 20% of climatological snowfall in coastal portions of Antarctica (Wille et al., 2021). In summer, AR precipitation sometimes falls as rain, particularly within the ablation zone (Mattingly et al., 2018). Combined with increased temperatures from enhanced cloud downward longwave radiation, condensational heating, and warm air advection, AR rain can drive extreme surface melt (Box et al., 2022; Bozkurt et al., 2021; Guan et al., 2016; Mattingly et al., 2020; Wille et al., 2019) and destabilization of ice shelves (Wille et al., 2022). Given their outsized influence on the SMB of modern-day ice sheets, it is possible ARs have had an important role in shaping ice sheet behavior throughout Earth's history.

At the Last Glacial Maximum (LGM; ~21,000 years ago), ice sheets covered much of northern North America poleward of ~40°N, Fennoscandia, the Patagonian Andes, and Greenland and Antarctica. The equatorward position of the ice sheets in North America, Europe, and South America relative to the high-latitude ice sheets of today suggests the LGM ice sheets may have interacted with ARs at a higher frequency than the modern-day ice sheets on Greenland and Antarctica. However, changes to the location of extratropical storm tracks at the LGM (Kutzbach & Wright, 1985; Laîné et al., 2009; Lora et al., 2017; Oster et al., 2015; Tabor et al., 2021), in part driven by the ice sheets themselves (Löfverström et al., 2014), may have limited ice sheet AR landfalls. Similarly, stationary wave patterns, baroclinicity, Rossby wave breaking, and ocean evaporation, all of which

have been linked to AR characteristics today (Algarra et al., 2020; Baggett et al., 2016; Michel et al., 2021; Payne et al., 2020; Payne & Magnusdottir, 2014), were different at the LGM (Amaya et al., 2022; Bush & Philander, 1999; Kageyama & Valdes, 2000; Li & Battisti, 2008; Löfverström, 2020; Lora et al., 2016; Merz et al., 2015; Roberts et al., 2019), likely altering AR behavior.

Changes to ARs have been put forth as a driving mechanism behind mid-latitude LGM hydroclimate changes (Löfverström, 2020; Lora, 2018; Lora et al., 2017; Tabor et al., 2021). In particular, ARs have been implicated in the relatively wet (southwest U.S.) and dry (northwest U.S.) LGM conditions inferred from speleothem (Oster & Kelley, 2016), lacustrine (Kirby et al., 2013), and pollen records (Bartlein et al., 2011; Cleator et al., 2020). While these studies point to an important role for ARs in LGM mid-latitude hydroclimate, an examination of AR influence on LGM ice sheets has not been explored. Here we use a simulation of LGM climate and an automated AR detection algorithm to examine AR characteristics and their contribution to ice sheet precipitation to better understand the role of ARs in past climate and the atmospheric processes that influence long-term ice sheet accumulation and melt.

2. Methods

2.1. Model Simulations

We use the Community Earth System Model version 2 (CESM2) (Danabasoglu et al., 2020) to simulate LGM and preindustrial climates. The configuration of CESM2 employed here uses the Community Atmosphere Model version 5 (CAM5) (Neale et al., 2012), the Community Land Model version 5 (CLM5) with satellite phenology (Lawrence et al., 2019), the Parallel Ocean Program version 2 (POP2) (Smith et al., 2010), and the Los Alamos Sea Ice Model version 5.1.2 (CICE5.1.2) (Hunke et al., 2015). The land and atmosphere models have a horizontal resolution of 0.9° × 1.25°, and the ocean and sea ice models have a nominal 1° horizontal resolution.

The LGM simulation uses boundary conditions consistent with known LGM climate forcings following PMIP4 protocol (Kageyama et al., 2017), including LGM greenhouse gas concentrations and insolation values. Land ice sheets for the LGM simulation are prescribed using the ICE-6G reconstruction at 21 ka (Peltier et al., 2015), and include changes to surface albedo and elevation. Coastlines are also modified to account for ice sheet-induced changes in global sea level (Figure S1 in Supporting Information S1). The preindustrial simulation uses boundary conditions consistent with known climate forcings from the year 1850. Both simulations use aerosol emissions from the preindustrial period and prescribed climatological monthly varying satellite-derived vegetation distributions from the modern day. The LGM (preindustrial) simulation is initialized from year 500 (year 300) of the identical CESM2 LGM (preindustrial) simulation described in Zhu et al. (2021) and spun up for an additional 70 (125) years. After spin-up, the preindustrial and LGM simulations are run for an additional 100 years. The analysis presented here is based on these final 100 years from each simulation.

Equilibrium climate sensitivity within this configuration of CESM2 (with CAM5) is lower than that of the standard CESM2 with CAM6 (4.0 vs. 5.6°C, calculated in a slab ocean configuration) (Zhu et al., 2021). Global mean surface temperature in the LGM simulation is 8.98°C, 6.7°C colder than the preindustrial simulation (Figure S2 in Supporting Information S1), consistent with estimates from proxy-constrained reanalysis (Osman et al., 2021) and situated at the cooler end of estimates from the ensemble of PMIP4 models (PMIP4 min = −7.17°C; max = −3.26°C) (Kageyama et al., 2021).

2.2. Atmospheric River Identification

ARs are identified using an automated algorithm based on that of Lora et al. (2017), and used in previous climate change studies (Baek & Lora, 2021; Menemenlis et al., 2021; Skinner et al., 2020). ARs are defined as contiguous regions, at least 2,000 km in length, in which 6-hourly column integrated vapor transport (IVT) exceeds a threshold value. IVT is calculated as

$$\mathrm{IVT} = -\frac{1}{g}\int_{p_s}^{0} \boldsymbol{u} q \, dp$$

where $\boldsymbol{u}$, q, p are the horizontal winds, specific humidity, and pressure at each vertical model level, respectively, and g and p_s are the acceleration due to gravity and the surface pressure. The threshold value is based on zonal-mean integrated water vapor (IWV), and ARs are detected when

$$\mathrm{IVT} \geq \mathrm{IVT}_{\mathrm{min}}\left(1 - \frac{\overline{\mathrm{IWV}}}{\max\left(\overline{\mathrm{IWV}}\right)}\right)^{-1}$$

where $\overline{\mathrm{IWV}}$ is the 30-day running mean of the zonally-averaged IWV, $\max\left(\overline{\mathrm{IWV}}\right)$ is its latitudinal maximum, and $\mathrm{IVT}_{\mathrm{min}}$ is equal to 225 kg m^{-1} s^{-1}. The algorithm incorporates aspects of both absolute threshold-based ($\mathrm{IVT}_{\mathrm{min}}$) and relative (use of background IWV) detection methodologies (see Lora et al., 2020; Rutz et al., 2019).

Following Skinner et al. (2020), AR frequencies are calculated as the percentage of 6-hourly time steps in which an AR is detected divided by the total number of 6-hourly time steps in the specified analysis period. Precipitation from ARs is calculated as the sum of precipitation during the 6-hr time period in which the AR is detected. The same method is used to calculate AR-derived rain and snow. Temperature during ARs is calculated as the daily average temperature on days in which an AR is detected.

2.3. Ice Sheet Surface Mass Balance

We use a basic positive degree-day (PDD) scheme based on Pollard and DeConto (2012) to get a first order estimate of the change in ice sheet SMB induced by ARs. Daily mean 2-m temperature values on AR days are used to calculate an annual sum of daily temperatures above 0°C (positive degree day sum). Following Pollard and DeConto (2012), the degree day sum is multiplied by a melt coefficient of 0.005 m°C^{-1} day^{-1}, representing 0.005 m of melt per positive degree day. The calculated annual melt is then subtracted from the total AR-derived annual accumulated snowfall to quantify the change in ice sheet surface mass from ARs. The simplified scheme does not account for spatial variations in the melt coefficient or for the refreezing of meltwater. It also does not explicitly account for the melt induced by liquid precipitation associated with ARs.

3. Results

3.1. LGM AR Frequency and Relationship to the Large-Scale Environment

Annual AR frequency increases from the LGM to the preindustrial across much of the midlatitudes (Figure 1). Compared with PI, LGM ARs are 6%–14% less frequent across most of the North and South Pacific and Atlantic basins, and upwards of 16% less frequent across portions of the Southern Ocean (Figure 1b). The only region with greater AR activity during the LGM is the midlatitude North Atlantic (~35°N) south of the preindustrial period AR frequency maximum. Reductions in AR activity at the LGM extend from the ocean basins onto land, including across western and eastern North America, Europe, Southeast Asia, southern South America, and New Zealand. Despite reduced frequency, ARs do make landfall across each of these terrestrial regions during the LGM, and often impact the margins of the contemporaneous ice sheets (Figure 1a).

In North America, ARs are located over the coastal Cordilleran ice sheet 2%–6% of the time (percent of 6-hourly timesteps; see Methods) and over the eastern Laurentide ice sheet 2%–18% of the time. In Europe, South America, and New Zealand, ARs impact the coastal Fennoscandian, Patagonian, and Southern Alps ice sheets 2%–10% of the time. ARs are infrequent along the coastal Antarctic and Greenland ice sheets during the LGM, occurring less than 2% of the time. Equatorward of the ice sheets, ARs impact western North America 2%–6% of timesteps, eastern North America 2%–12% of timesteps, western Europe 2%–14% of timesteps, east Asia 2%–10% of timesteps, and New Zealand 2%–6% of timesteps. Apart from the Iberian Peninsula, all these AR frequency values are lower than those in the preindustrial period (Figure 1b).

AR frequency changes since the LGM are consistent with changes in large-scale circulation and atmospheric moisture. In the Southern Hemisphere and North Pacific, changes to the eddy-driven jets are small with no clear latitudinal shift in the location of the jet core (Figures 2a and 2b). The relatively small changes to zonal flow in the Pacific and Southern Hemisphere in CESM are robust across most PMIP4 models (Kageyama et al., 2021). The reduction in AR frequency in these regions is likely driven in large part by a drier atmosphere during the cold

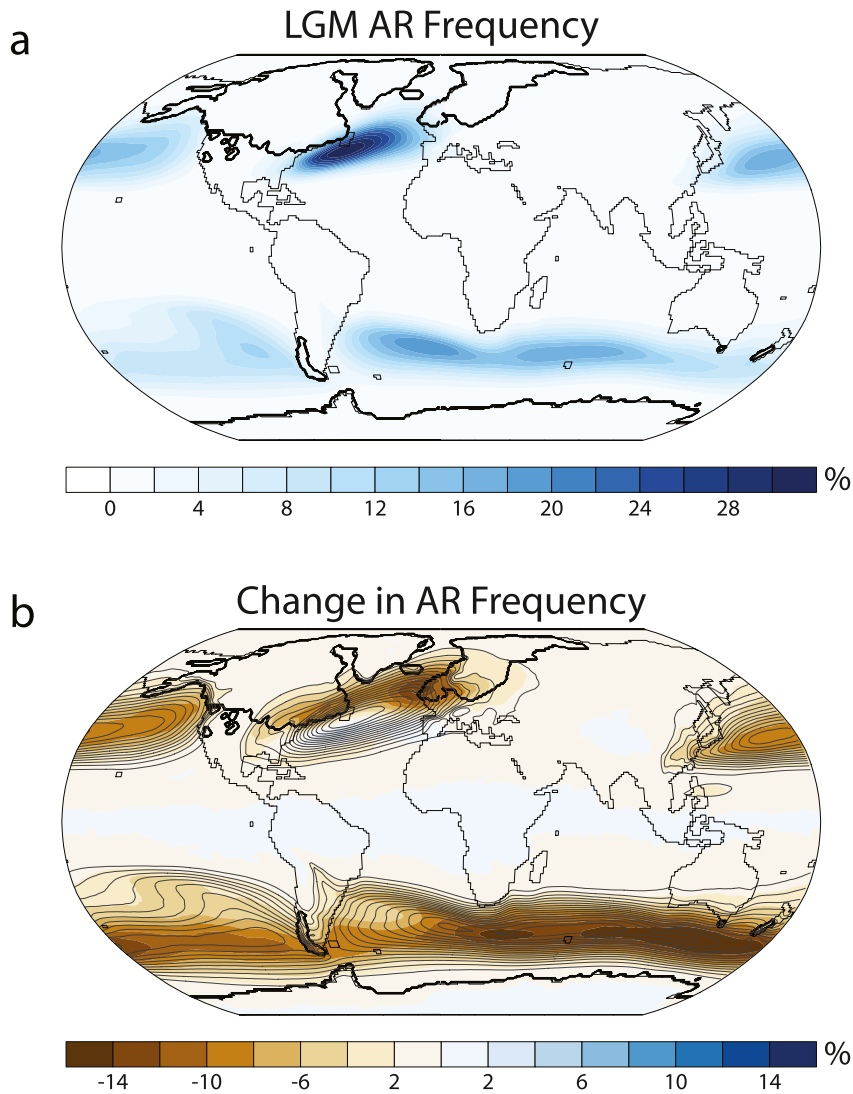

Figure 1. Last Glacial Maximum (LGM) atmospheric river (AR) frequency and change. (a) Annual AR frequency during the LGM. (b) Change in annual AR frequency (colors) between the LGM and preindustrial periods (LGM—Preindustrial), and preindustrial period AR frequency (gray contours; spacing from 0 to 30 percent). Frequency is defined as the percentage of all 6-hourly timesteps in which an AR is detected. The thick black contour lines indicate the edges of the LGM ice sheets.

LGM (Figure 2c). In the North Atlantic, the eddy-driven jet narrows and increases in strength, consistent with an enhanced surface temperature gradient (Figure S2 in Supporting Information S1) and enhanced stationary wave momentum flux convergence associated with the Laurentide ice sheet (Kageyama & Valdes, 2000; Löfverström et al., 2016; Merz et al., 2015). AR frequency increases in this region of the North Atlantic despite reductions in atmospheric moisture, pointing to the important role of the enhanced stationary wave pattern and baroclinicity for increased AR development (e.g., Löfverström, 2020; Menemenlis et al., 2021).

3.2. LGM AR Precipitation, Temperature, and Impact on Surface Mass Balance

Simulated precipitation change between the LGM and preindustrial in CESM (Figure S3a in Supporting Information S1) resembles that of the PMIP4 multi-model mean (Kageyama et al., 2021) and is largely consistent with pollen-based proxy records of LGM hydroclimate (Bartlein et al., 2011; Cleator et al., 2020). Greatest precipitation reductions at the LGM are located over the ice sheets, where anticyclonic circulation is common (Bush & Philander, 1999; Lora, 2018), and over the Indo-Pacific warm pool in response to continental shelf exposure and a weaker Walker Circulation (DiNezio et al., 2018). With some exceptions, drier LGM conditions are also present

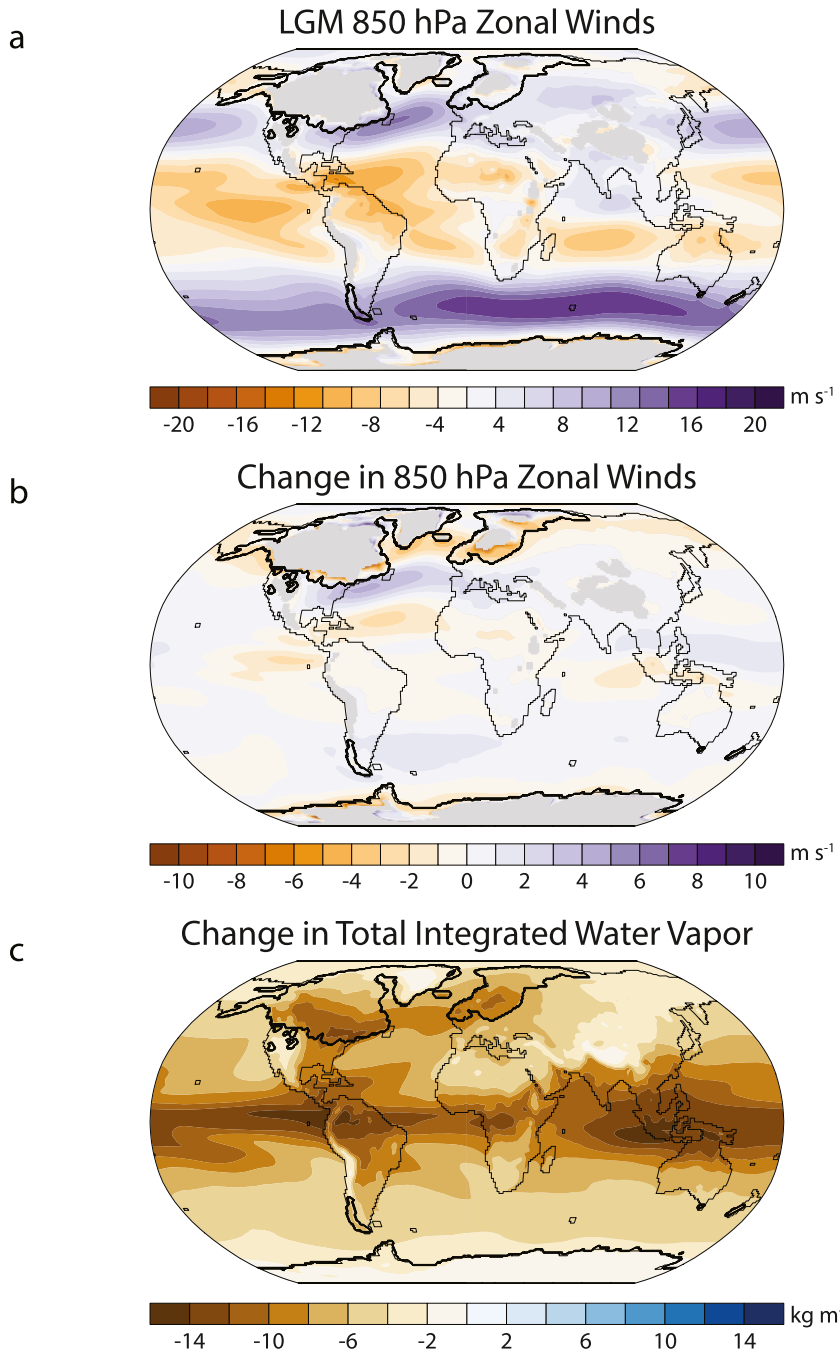

Figure 2. Atmospheric conditions relevant for Last Glacial Maximum (LGM) atmospheric rivers. (a) LGM annual mean 850 hPa zonal wind. (b) Change in the annual mean 850 hPa zonal wind between the LGM and preindustrial (LGM—Preindustrial). (c) Change in the annual mean total integrated water vapor between the LGM and preindustrial.

on unglaciated continental areas. Overall agreement between the simulated total precipitation change in CESM and other climate models (Kageyama et al., 2021) suggests that the AR-driven precipitation changes discussed next are robust.

ARs are responsible for a considerable portion of total LGM precipitation along the margins of the Northern and Southern Hemisphere ice sheets (Figures 3a–3c). ARs are particularly instrumental in supplying precipitation along the eastern Laurentide ice sheet, where they deposit as much as 1,300 mm/year and contribute up to 53% of all precipitation (interquartile range (IQR) of 10%–27%). Along the western Fennoscandian and Cordilleran

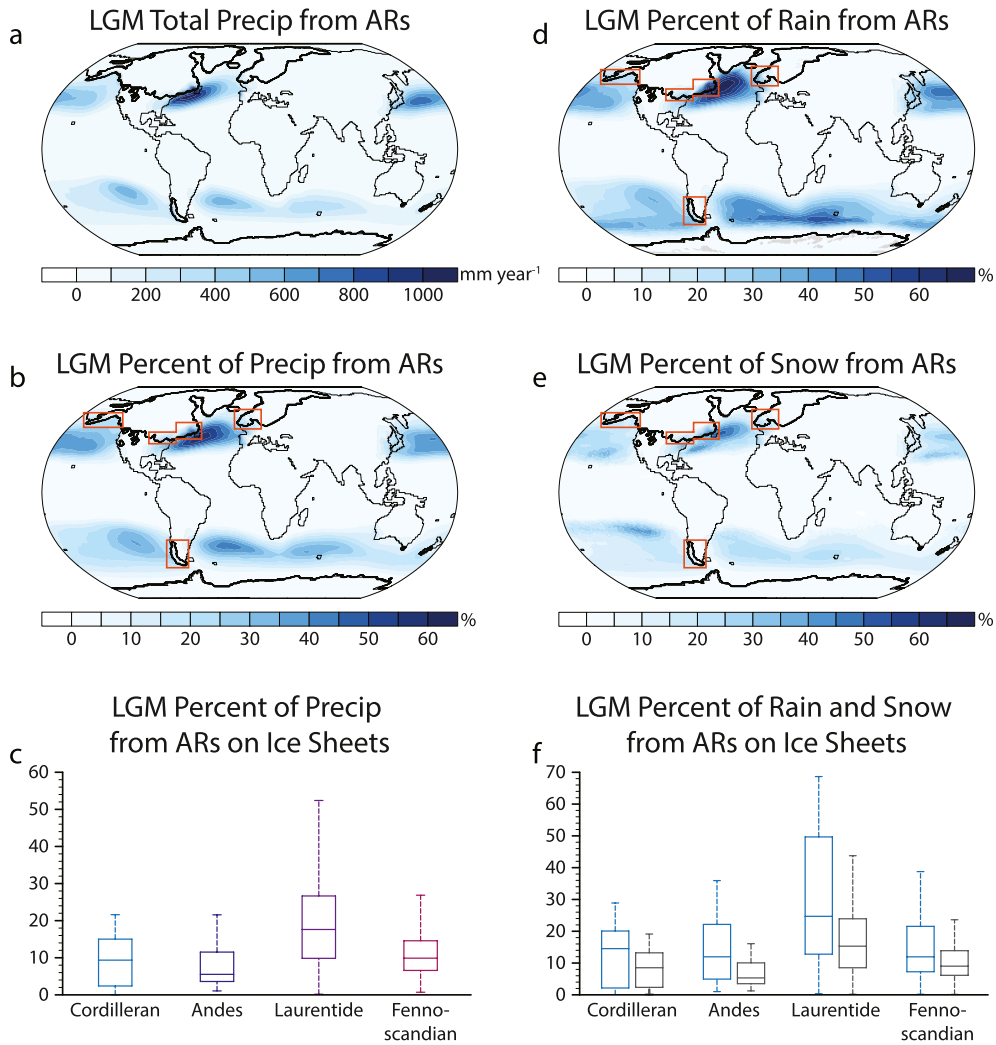

Figure 3. Last Glacial Maximum (LGM) precipitation from atmospheric rivers (ARs). (a) LGM total annual precipitation from ARs. (b, d, e) Percentage of all (b) precipitation, (d) rain, and (e) snow from ARs. (c, f) Boxplots (min, IQR, max) of the percentage of all (c) precipitation, and (f) rain (blue) and snow (gray) from ARs over the ice sheet areas marked in orange in (b, d, e).

ice sheets, ARs are responsible for as much as 350 mm/year and 400 mm/year, respectively, corresponding to a maximum of 27% and 22% of all precipitation (IQR of 7%–15% and 3%–15%) (Figure 3c). In Patagonia, AR precipitation reaches 700 mm/year and contributes up to 22% of all precipitation (IQR of 4%–12%). In contrast, AR contributions to LGM Antarctic and Greenland precipitation are minimal, accounting for less than 5% of annual precipitation.

Though not the focus here, ARs are also important contributors to precipitation in non-glaciated regions of western and eastern North America, western Europe, east Asia, and New Zealand during the LGM (Figures 3a and 3b). A comparison between the simulated change in AR-based precipitation (Figure S3b in Supporting Information S1) and total precipitation (Figure S3a in Supporting Information S1) indicates that ARs are largely responsible for the increase in total LGM precipitation in the Iberian Peninsula (e.g., Beghin et al., 2016; Löfverström & Lora, 2017), but not responsible for the increase in LGM precipitation in the Southwestern U.S. (counter to our expectations; e.g., Kirby et al., 2013; Lora et al., 2017). We note that the difference between the AR response to LGM forcings over the Southwestern U.S. presented here and in prior studies with PMIP3 models is not the result of different AR algorithms, and reflects differences in simulated climate that will be explored in future work.

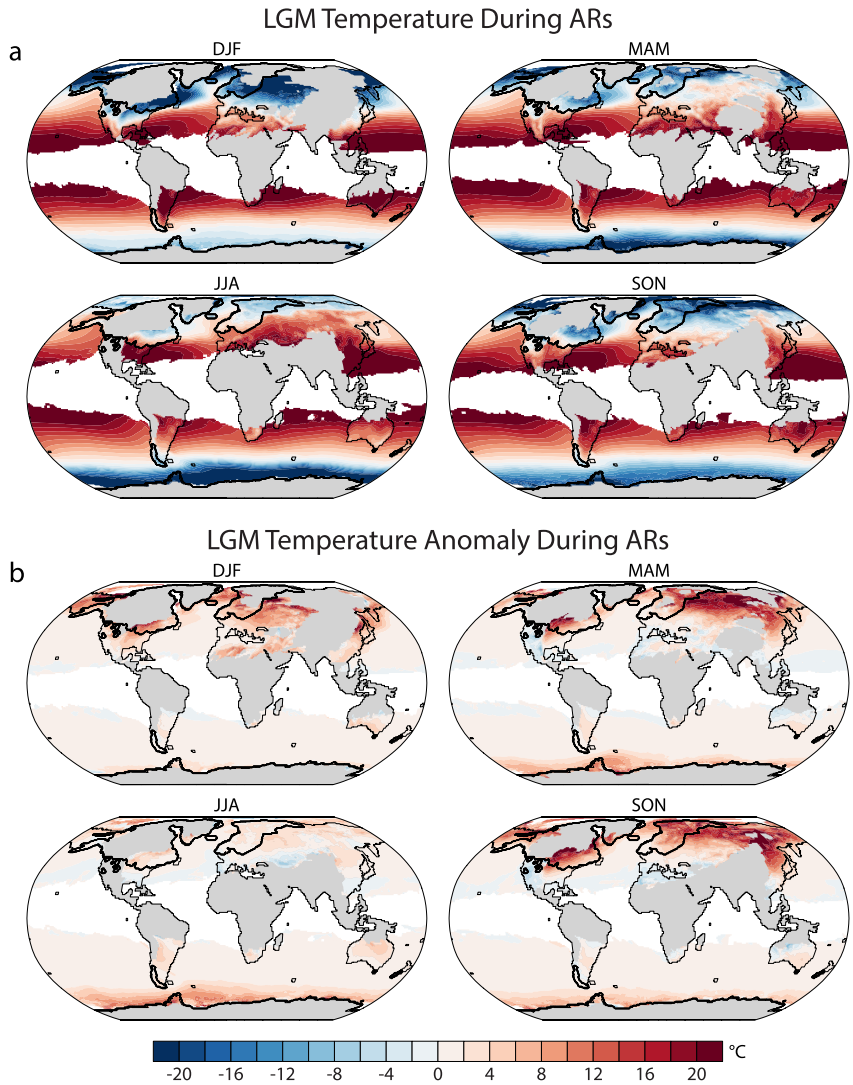

Figure 4. Temperature during Last Glacial Maximum (LGM) atmospheric rivers (ARs). (a) Average 2-m temperature during LGM AR events in each season. (b) Average anomaly in 2-m temperature during LGM AR events in each season. Gray/white grid cells indicate no AR events over land/ocean, respectively.

AR precipitation falls as both rain and snow along the LGM ice sheets (Figures 3d–3f). Annually, ARs provide up to 44% of all snow and 69% of all rain along the eastern Laurentide ice sheet (IQR of 9–24% and 13–50%), 22% of all snow and 39% of all rain along the western Fennoscandian ice sheet (IQR of 6–14% and 7–22%), 19% of all snow and 29% of all rain along the western Cordilleran ice sheet (IQR of 2%–13% and 2%–20%), and 16% of all snow and 36% of all rain along the Andes ice sheet (IQR of 3%–10% and 5%–22%) (Figure 3f). In winter and spring, nearly all AR-derived precipitation on the ice sheets is in the form of snow (Figure S4 in Supporting Information S1). In summer and fall, ARs supply a considerable amount of rainfall, particularly along coastal stretches of the eastern Laurentide and western Cordilleran ice sheets (Figure S4 in Supporting Information S1).

ARs are associated with flow from lower latitudes and anomalously warm temperatures over ice sheets (Figure 4). In winter, spring, and fall, near-surface temperatures on days with an AR are often 10–20°C above average over the eastern Laurentide and Fennoscandian ice sheets (Figure 4b). During summer, AR temperature anomalies are smaller, ranging from just below 0–7°C. Despite anomalously warm conditions, temperatures near the surface during AR events in winter and spring remain below freezing, and therefore support snowfall and ice sheet accumulation (Figure S4 in Supporting Information S1, Figure 4a). During fall, AR temperatures along coastal stretches of all ice sheets as well as interior portions of the southern Laurentide ice sheet exceed the freezing

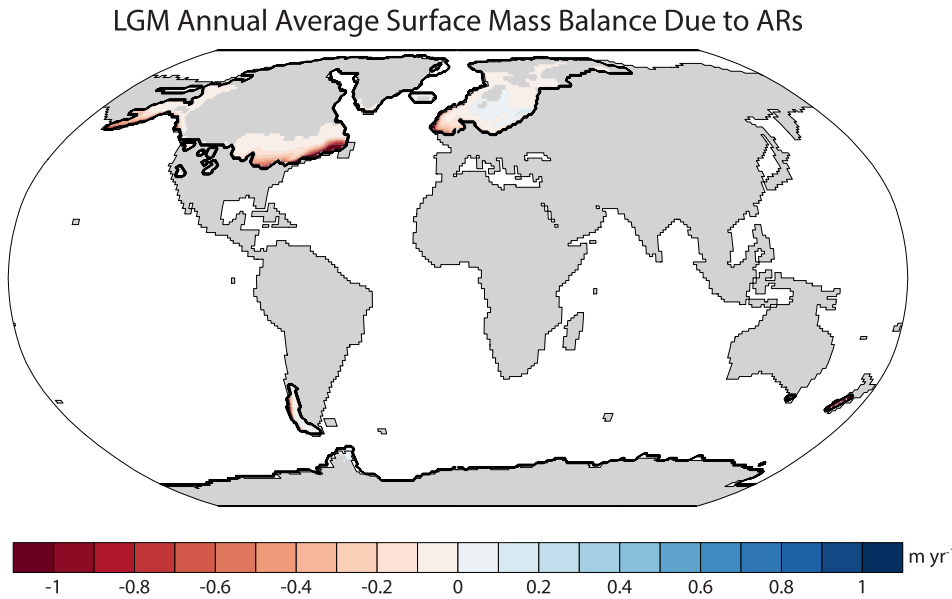

Figure 5. Annual average surface mass balance induced by atmospheric rivers (see Methods) at the Last Glacial Maximum.

point. Similarly, in summer, AR temperatures often exceed the freezing point across large portions of ice sheets in both hemispheres. These relatively warm temperatures allow for liquid precipitation (Figure S4 in Supporting Information S1), and the potential for substantial surface melt during AR events. Indeed, calculations of SMB induced by ARs (see Methods) suggest that melting from ARs exceeds snowfall accumulation across most ice sheet areas (Figure 5). This is especially the case along coastal regions of each ice sheet, where AR temperatures are often near or above freezing outside of winter.

4. Discussion and Conclusion

The simulations presented here indicate ARs were important contributors to ice sheet surface mass and energy fluxes at the LGM. The substantial equatorward extension of the ice sheets into the high middle latitudes combined with only minor displacement of the mid-latitude storm tracks from today promotes frequent AR landfalls along the ice sheet margins. Though increasingly recognized as important divers of accumulation and melt in modern day Antarctica and Greenland, the results suggest ARs have had an even greater role in ice sheet hydroclimate in Earth's past.

The net annual SMB at the LGM is expected to be relatively small (Pollard & Thompson, 1997), and the counteracting contributions from ARs in the cold seasons (snow accumulation) and warm seasons (rain and above freezing temperatures), is consistent with this expectation. Our use of a simplified PDD SMB scheme indicates ARs drove more melt than accumulation along LGM ice sheet margins. It is possible that the melt associated with ARs, along with other processes, served to limit further equatorward movement of the ice sheet margins in some locations at the LGM. While greater AR-induced melt along the edges of the ice sheets is plausible given the expected warmer temperatures within the poleward directed flow of ARs, it is worth noting that the PDD scheme is a simplified representation of SMB, and because the position of the ice sheets is fixed in the simulation, the ice sheet is not necessarily in equilibrium with the simulated climate. With regards to the latter point, this means that the atmospheric state simulated in CESM may be too warm to support ice sheets at the prescribed margins, which may artificially skew the contribution of ARs toward melting in our analysis. Climate-ice sheet mismatches are a potential issue with all PMIP simulations (Alder & Hostetler, 2019; Pollard, 2000), and to fully assess the impact of ARs on ice sheet mass balance and subsequent ice sheet movement will require use of a dynamic ice sheet model.

During periods of ice sheet growth and retreat, ARs may have had a more pronounced role in positive and negative ice sheet SMB, respectively. For example, it is plausible that the relatively rapid Laurentide ice sheet advance during the Late Wisconsin period preceding the LGM (Dyke et al., 2002) was aided along the southwest and

southeast margins by AR-driven snow. Northern Hemisphere (NH) summer insolation was weaker in the years prior to the LGM, which likely would have increased the fraction of warm season AR precipitation that fell as snow relative to the LGM. Similarly, the progression to greater NH summer insolation following the LGM likely led to more AR-induced ice sheet melt events, which may have created the conditions necessary for accelerated ice sheet flow. During surface melt events, meltwater from the ablation zone can drain to the base of the ice sheet, increasing basal sliding and the retreat of ice sheet margins (Doyle et al., 2015; Zwally et al., 2002). Zwally et al. (2002) and Bromwich et al. (2005) have suggested that surface melt may have accelerated Laurentide ice movement. ARs may have served as a key atmospheric mechanism driving this ice sheet retreat following the LGM.

Differences in AR characteristics between the LGM and preindustrial highlight the sensitivity of ARs to background climate state, consistent with previous AR studies of past (Lora et al., 2017; Menemenlis et al., 2021; Shields et al., 2021; Skinner & Poulsen, 2016; Skinner et al., 2020; Tabor et al., 2021) and projected future climates (Baek & Lora, 2021; O'Brien et al., 2022; Payne et al., 2020). Cold temperatures and the associated reduction in evaporation and atmospheric moisture at the LGM result in fewer ARs in our simulations, and less AR-derived precipitation across most of the Northern and Southern extratropics compared with the modern day. Interestingly, despite a drier atmosphere in the North Atlantic (Figure 2c), AR frequency and AR precipitation is greater along a large portion of the mid-latitude North Atlantic and coastal Iberian Peninsula in response to enhanced regional baroclinicity during the LGM (Kageyama & Valdes, 2000), highlighting the possibility of enhanced AR activity during cooler climates given sufficient dynamical forcing.

While direct evidence for AR influence on LGM ice sheet precipitation, for example, in ice cores, is limited or unavailable, proxies from near the ice margins, combined with the AR analysis presented here provide insights into the atmospheric mechanisms that shaped hydroclimate in these areas. For example, pollen records from marine sediments west of the Patagonian ice sheet suggest considerably wetter conditions at the LGM (Berman et al., 2016). CESM simulates an increase in overall LGM precipitation in this area, but a decrease in AR-derived precipitation (Figure S3 in Supporting Information S1), suggesting that, while ARs were an important contributor to Patagonian ice sheet precipitation, other atmospheric systems were responsible for the substantial increase in regional precipitation. In Europe, speleothems from the Alps suggest southerly moisture transport at the LGM (Luetscher et al., 2015; Spötl et al., 2021), consistent with a considerable role for ARs in the Alps and just to the north along the margin of the Fennoscandian ice sheet, as simulated here.

Agreement between mid-latitude LGM precipitation in CESM and other models from PMIP4 (Kageyama et al., 2021) suggests that the response of ARs to LGM climate forcings may be robust across models. However, explicitly examining ARs across the PMIP4 ensemble is not feasible due to limited availability of the necessary high frequency, three-dimensional variables. As noted earlier, simulated LGM climate in CESM is relatively cold compared with other models (and some reconstructions (e.g., Annan et al., 2022)), and it is possible that AR detection would be higher in those other LGM simulations. Additional uncertainty in our results derives from the use of a single AR detection algorithm (Rutz et al., 2019), though detection algorithms tend to identify medium- and high-intensity ARs similarly (Lora et al., 2020). Future planned work will examine the robustness of paleo AR changes to a suite of AR detection algorithms (Shields et al., 2018).

Data Availability Statement

CESM2 model code is available at https://www.cesm.ucar.edu/models/cesm2/release_download.html. Relevant data, including the AR catalogs and CESM output from the simulations, is archived on Zenodo at the following DOI: https://doi.org/10.5281/zenodo.7339985.

Acknowledgments
This work was supported by National Science Foundation Awards 1903600 and AGS-1903528. The CESM project is supported primarily by the National Science Foundation (NSF). This material is based upon work supported by the National Center for Atmospheric Research, which is a major facility sponsored by the NSF under Cooperative Agreement No. 1852977. Computing and data storage resources, including the Cheyenne supercomputer (https://doi.org/10.5065/D6RX99HX), were provided by the Computational and Information Systems Laboratory (CISL) at NCAR.

References

Alder, J. R., & Hostetler, S. W. (2019). Applying the Community Ice Sheet Model to evaluate PMIP3 LGM climatologies over the North American ice sheets. *Climate Dynamics*, *53*(5), 2807–2824. https://doi.org/10.1007/s00382-019-04663-x

Algarra, I., Nieto, R., Ramos, A. M., Eiras-Barca, J., Trigo, R. M., & Gimeno, L. (2020). Significant increase of global anomalous moisture uptake feeding landfalling atmospheric rivers. *Nature Communications*, *11*(1), 5082. https://doi.org/10.1038/s41467-020-18876-w

Amaya, D. J., Seltzer, A. M., Karnauskas, K. B., Lora, J. M., Zhang, X., & DiNezio, P. N. (2022). Air-sea coupling shapes North American hydroclimate response to ice sheets during the Last Glacial Maximum. *Earth and Planetary Science Letters*, *578*, 117271. https://doi.org/10.1016/j.epsl.2021.117271

Annan, J. D., Hargreaves, J. C., & Mauritsen, T. (2022). A new global surface temperature reconstruction for the Last Glacial Maximum. *Climate of the Past*, *18*(8), 1883–1896. https://doi.org/10.5194/cp-18-1883-2022

Baek, S. H., & Lora, J. M. (2021). Counterbalancing influences of aerosols and greenhouse gases on atmospheric rivers. *Nature Climate Change*, *11*(11), 958–965. https://doi.org/10.1038/s41558-021-01166-8

Baggett, C., Lee, S., & Feldstein, S. (2016). An investigation of the presence of atmospheric rivers over the North Pacific during planetary-scale wave life cycles and their role in Arctic warming. *Journal of the Atmospheric Sciences*, *73*(11), 4329–4347. https://doi.org/10.1175/jas-d-16-0033.1

Bartlein, P. J., Harrison, S. P., Brewer, S., Connor, S., Davis, B. A. S., Gajewski, K., et al. (2011). Pollen-based continental climate reconstructions at 6 and 21 ka: A global synthesis. *Climate Dynamics*, *37*(3), 775–802. https://doi.org/10.1007/s00382-010-0904-1

Beghin, P., Charbit, S., Kageyama, M., Combourieu-Nebout, N., Hatté, C., Dumas, C., & Peterschmitt, J. Y. (2016). What drives LGM precipitation over the western Mediterranean? A study focused on the Iberian Peninsula and northern Morocco. *Climate Dynamics*, *46*(7), 2611–2631. https://doi.org/10.1007/s00382-015-2720-0

Berman, A. L., Silvestri, G. E., & Tonello, M. S. (2016). Differences between Last Glacial Maximum and present-day temperature and precipitation in southern South America. *Quaternary Science Reviews*, *150*, 221–233. https://doi.org/10.1016/j.quascirev.2016.08.025

Box, J. E., Wehrlé, A., van As, D., Fausto, R. S., Kjeldsen, K. K., Dachauer, A., et al. (2022). Greenland Ice Sheet Rainfall, heat and albedo feedback impacts from the Mid-August 2021 atmospheric river. *Geophysical Research Letters*, *49*(11), e2021GL097356. https://doi.org/10.1029/2021GL097356

Bozkurt, D., Sen, O. L., Ezber, Y., Guan, B., Viale, M., & Caglar, F. (2021). Influence of African atmospheric rivers on precipitation and snowmelt in the near East's highlands. *Journal of Geophysical Research: Atmospheres*, *126*(4), e2020JD033646. https://doi.org/10.1029/2020JD033646

Bromwich, D. H., Toracinta, E. R., Oglesby, R. J., Fastook, J. L., & Hughes, T. J. (2005). LGM summer climate on the southern margin of the Laurentide Ice Sheet: Wet or dry? *Journal of Climate*, *18*(16), 3317–3338. https://doi.org/10.1175/jcli3480.1

Bush, A. B. G., & Philander, S. G. H. (1999). The climate of the Last Glacial Maximum: Results from a coupled atmosphere-ocean general circulation model. *Journal of Geophysical Research*, *104*(D20), 24509–24525. https://doi.org/10.1029/1999JD900447

Cleator, S. F., Harrison, S. P., Nichols, N. K., Prentice, I. C., & Roulstone, I. (2020). A new multivariable benchmark for Last Glacial Maximum climate simulations. *Climate of the Past*, *16*(2), 699–712. https://doi.org/10.5194/cp-16-699-2020

Dacre, H. F., Clark, P. A., Martinez-Alvarado, O., Stringer, M. A., & Lavers, D. A. (2015). How do atmospheric rivers form? *Bulletin of the American Meteorological Society*, *96*(8), 1243–1255. https://doi.org/10.1175/bams-d-14-00031.1

Danabasoglu, G., Lamarque, J. F., Bacmeister, J., Bailey, D. A., DuVivier, A. K., Edwards, J., et al. (2020). The Community Earth System Model version 2 (CESM2). *Journal of Advances in Modeling Earth Systems*, *12*(2), e2019MS001916. https://doi.org/10.1029/2019MS001916

DiNezio, P. N., Tierney, J. E., Otto-Bliesner, B. L., Timmermann, A., Bhattacharya, T., Rosenbloom, N., & Brady, E. (2018). Glacial changes in tropical climate amplified by the Indian Ocean. *Science Advances*, *4*(12), eaat9658. https://doi.org/10.1126/sciadv.aat9658

Doyle, S. H., Hubbard, A., van de Wal, R. S. W., Box, J. E., van As, D., Scharrer, K., et al. (2015). Amplified melt and flow of the Greenland ice sheet driven by late-summer cyclonic rainfall. *Nature Geoscience*, *8*(8), 647–653. https://doi.org/10.1038/ngeo2482

Dyke, A. S., Andrews, J. T., Clark, P. U., England, J. H., Miller, G. H., Shaw, J., & Veillette, J. J. (2002). The Laurentide and Innuitian ice sheets during the Last Glacial Maximum. *Quaternary Science Reviews*, *21*(1), 9–31. https://doi.org/10.1016/s0277-3791(01)00095-6

Gorodetskaya, I. V., Tsukernik, M., Claes, K., Ralph, M. F., Neff, W. D., & Van Lipzig, N. P. M. (2014). The role of atmospheric rivers in anomalous snow accumulation in East Antarctica. *Geophysical Research Letters*, *41*(17), 6199–6206. https://doi.org/10.1002/2014GL060881

Guan, B., Waliser, D. E., Ralph, F. M., Fetzer, E. J., & Neiman, P. J. (2016). Hydrometeorological characteristics of rain-on-snow events associated with atmospheric rivers. *Geophysical Research Letters*, *43*(6), 2964–2973. https://doi.org/10.1002/2016GL067978

Hunke, E. C., Lipscombe, W. H., Turner, A. K., Jeffery, N., & Elliot, S. (2015). *CICE: The Los Alamos sea ice model documentation and software user's manual, version 5.1*. LA-CC-06-012. Los Alamos National the Laboratory.

Kageyama, M., Albani, S., Braconnot, P., Harrison, S. P., Hopcroft, P. O., Ivanovic, R. F., et al. (2017). The PMIP4 contribution to CMIP6—Part 4: Scientific objectives and experimental design of the PMIP4-CMIP6 Last Glacial Maximum experiments and PMIP4 sensitivity experiments. *Geoscientific Model Development*, *10*(11), 4035–4055. https://doi.org/10.5194/gmd-10-4035-2017

Kageyama, M., Harrison, S. P., Kapsch, M. L., Lofverstrom, M., Lora, J. M., Mikolajewicz, U., et al. (2021). The PMIP4 Last Glacial Maximum experiments: Preliminary results and comparison with the PMIP3 simulations. *Climate of the Past*, *17*(3), 1065–1089. https://doi.org/10.5194/cp-17-1065-2021

Kageyama, M., & Valdes, P. J. (2000). Impact of the North American ice-sheet orography on the Last Glacial Maximum eddies and snowfall. *Geophysical Research Letters*, *27*(10), 1515–1518. https://doi.org/10.1029/1999GL011274

Kirby, M. E., Feakins, S. J., Bonuso, N., Fantozzi, J. M., & Hiner, C. A. (2013). Latest Pleistocene to Holocene hydroclimates from Lake Elsinore, California. *Quaternary Science Reviews*, *76*, 1–15. https://doi.org/10.1016/j.quascirev.2013.05.023

Kutzbach, J. E., & Wright, H. E. (1985). Simulation of the climate of 18,000 years BP: Results for the North American/North Atlantic/European sector and comparison with the geologic record of North America. *Quaternary Science Reviews*, *4*(3), 147–187. https://doi.org/10.1016/0277-3791(85)90024-1

Laîné, A., Kageyama, M., Salas-Mélia, D., Voldoire, A., Rivière, G., Ramstein, G., et al. (2009). Northern hemisphere storm tracks during the last glacial maximum in the PMIP2 ocean-atmosphere coupled models: Energetic study, seasonal cycle, precipitation. *Climate Dynamics*, *32*(5), 593–614. https://doi.org/10.1007/s00382-008-0391-9

Lawrence, D. M., Fisher, R. A., Koven, C. D., Oleson, K. W., Swenson, S. C., Bonan, G., et al. (2019). The Community Land Model version 5: Description of new features, benchmarking, and impact of forcing uncertainty. *Journal of Advances in Modeling Earth Systems*, *11*(12), 4245–4287. https://doi.org/10.1029/2018MS001583

Li, C., & Battisti, D. S. (2008). Reduced Atlantic storminess during Last Glacial Maximum: Evidence from a coupled climate model. *Journal of Climate*, *21*(14), 3561–3579. https://doi.org/10.1175/2007jcli2166.1

Löfverström, M. (2020). A dynamic link between high-intensity precipitation events in southwestern North America and Europe at the Last Glacial Maximum. *Earth and Planetary Science Letters*, *534*, 116081. https://doi.org/10.1016/j.epsl.2020.116081

Löfverström, M., Caballero, R., Nilsson, J., & Kleman, J. (2014). Evolution of the large-scale atmospheric circulation in response to changing ice sheets over the last glacial cycle. *Climate of the Past*, *10*(4), 1453–1471. https://doi.org/10.5194/cp-10-1453-2014

Löfverström, M., Caballero, R., Nilsson, J., & Messori, G. (2016). Stationary wave reflection as a mechanism for zonalizing the Atlantic winter jet at the LGM. *Journal of the Atmospheric Sciences*, *73*(8), 3329–3342. https://doi.org/10.1175/jas-d-15-0295.1

Löfverström, M., & Lora, J. M. (2017). Abrupt regime shifts in the North Atlantic atmospheric circulation over the last deglaciation. *Geophysical Research Letters*, *44*(15), 8047–8055. https://doi.org/10.1002/2017GL074274

Lora, J. M. (2018). Components and mechanisms of hydrologic cycle changes over North America at the Last Glacial Maximum. *Journal of Climate*, *31*(17), 7035–7051. https://doi.org/10.1175/jcli-d-17-0544.1

Lora, J. M., Mitchell, J. L., Risi, C., & Tripati, A. E. (2017). North Pacific atmospheric rivers and their influence on western North America at the Last Glacial Maximum. *Geophysical Research Letters*, *44*(2), 1051–1059. https://doi.org/10.1002/2016GL071541

Lora, J. M., Mitchell, J. L., & Tripati, A. E. (2016). Abrupt reorganization of North Pacific and western North American climate during the last deglaciation. *Geophysical Research Letters*, *43*(22), 11–796. https://doi.org/10.1002/2016GL071244

Lora, J. M., Shields, C. A., & Rutz, J. J. (2020). Consensus and disagreement in atmospheric river detection: ARTMIP global catalogues. *Geophysical Research Letters*, *47*(20), e2020GL089302. https://doi.org/10.1029/2020GL089302

Luetscher, M., Boch, R., Sodemann, H., Spötl, C., Cheng, H., Edwards, R. L., et al. (2015). North Atlantic storm track changes during the Last Glacial Maximum recorded by Alpine speleothems. *Nature Communications*, *6*(1), 6344. https://doi.org/10.1038/ncomms7344

Mattingly, K. S., Mote, T. L., & Fettweis, X. (2018). Atmospheric river impacts on Greenland Ice Sheet surface mass balance. *Journal of Geophysical Research: Atmospheres*, *123*(16), 8538–8560. https://doi.org/10.1029/2018JD028714

Mattingly, K. S., Mote, T. L., Fettweis, X., van As, D., Van Tricht, K., Lhermitte, S., et al. (2020). Strong summer atmospheric rivers trigger Greenland Ice Sheet melt through spatially varying surface energy balance and cloud regimes. *Journal of Climate*, *33*(16), 6809–6832. https://doi.org/10.1175/jcli-d-19-0835.1

Menemenlis, S., Lora, J. M., Lofverstrom, M., & Chandan, D. (2021). Influence of stationary waves on mid-Pliocene atmospheric rivers and hydroclimate. *Global and Planetary Change*, *204*, 103557. https://doi.org/10.1016/j.gloplacha.2021.103557

Merz, N., Raible, C. C., & Woollings, T. (2015). North Atlantic eddy-driven jet in interglacial and glacial winter climates. *Journal of Climate*, *28*(10), 3977–3997. https://doi.org/10.1175/jcli-d-14-00525.1

Michel, C., Sorteberg, A., Eckhardt, S., Weijenborg, C., Stohl, A., & Cassiani, M. (2021). Characterization of the atmospheric environment during extreme precipitation events associated with atmospheric rivers in Norway—Seasonal and regional aspects. *Weather and Climate Extremes*, *34*, 100370. https://doi.org/10.1016/j.wace.2021.100370

Neale, R. B., Garcia, R., Kinnison, D., Lamarque, J. F., Marsh, D., Mills, M., et al. (2012). *Description of the NCAR community atmosphere model (CAM 5.0), Tech. Rep*. National Center for Atmospheric Research.

Neff, W., Compo, G. P., Martin Ralph, F., & Shupe, M. D. (2014). Continental heat anomalies and the extreme melting of the Greenland ice surface in 2012 and 1889. *Journal of Geophysical Research: Atmospheres*, *119*(11), 6520–6536. https://doi.org/10.1002/2014JD021470

O'Brien, T. A., Wehner, M. F., Payne, A. E., Shields, C. A., Rutz, J. J., Leung, L. R., et al. (2022). Increases in future AR count and size: Overview of the ARTMIP tier 2 CMIP5/6 experiment. *Journal of Geophysical Research: Atmospheres*, *127*(6), e2021JD036013. https://doi.org/10.1029/2021JD036013

Osman, M. B., Tierney, J. E., Zhu, J., Tardif, R., Hakim, G. J., King, J., & Poulsen, C. J. (2021). Globally resolved surface temperatures since the Last Glacial Maximum. *Nature*, *599*(7884), 239–244. https://doi.org/10.1038/s41586-021-03984-4

Oster, J. L., Ibarra, D. E., Winnick, M. J., & Maher, K. (2015). Steering of westerly storms over western North America at the Last Glacial Maximum. *Nature Geoscience*, *8*(3), 201–205. https://doi.org/10.1038/ngeo2365

Oster, J. L., & Kelley, N. P. (2016). Tracking regional and global teleconnections recorded by western North American speleothem records. *Quaternary Science Reviews*, *149*, 18–33. https://doi.org/10.1016/j.quascirev.2016.07.009

Payne, A. E., Demory, M.-E., Leung, L. R., Ramos, A. M., Shields, C. A., Rutz, J. J., et al. (2020). Responses and impacts of atmospheric rivers to climate change. *Nature Reviews Earth & Environment*, *1*(3), 143–157. https://doi.org/10.1038/s43017-020-0030-5

Payne, A. E., & Magnusdottir, G. (2014). Dynamics of landfalling atmospheric rivers over the North Pacific in 30 years of MERRA reanalysis. *Journal of Climate*, *27*(18), 7133–7150. https://doi.org/10.1175/jcli-d-14-00034.1

Peltier, W. R., Argus, D. F., & Drummond, R. (2015). Space geodesy constrains ice age terminal deglaciation: The global ICE-6G_C (VM5a) model. *Journal of Geophysical Research: Solid Earth*, *120*(1), 450–487. https://doi.org/10.1002/2014JB011176

Pollard, D. (2000). Comparisons of ice-sheet surface mass budgets from Paleoclimate Modeling Intercomparison Project (PMIP) simulations. *Global and Planetary Change*, *24*(2), 79–106. https://doi.org/10.1016/s0921-8181(99)00071-5

Pollard, D., & DeConto, R. M. (2012). Description of a hybrid ice sheet-shelf model, and application to Antarctica. *Geoscientific Model Development*, *5*(5), 1273–1295. https://doi.org/10.5194/gmd-5-1273-2012

Pollard, D., & Thompson, S. L. (1997). Climate and ice-sheet mass balance at the last glacial maximum from the GENESIS version 2 global climate model. *Quaternary Science Reviews*, *16*(8), 841–863. https://doi.org/10.1016/s0277-3791(96)00115-1

Roberts, W. H. G., Li, C., & Valdes, P. J. (2019). The mechanisms that determine the response of the Northern Hemisphere's stationary waves to North American Ice Sheets. *Journal of Climate*, *32*(13), 3917–3940. https://doi.org/10.1175/jcli-d-18-0586.1

Rutz, J. J., Shields, C. A., Lora, J. M., Payne, A. E., Guan, B., Ullrich, P., et al. (2019). The atmospheric river tracking method intercomparison project (ARTMIP): Quantifying uncertainties in atmospheric river climatology. *Journal of Geophysical Research: Atmospheres*, *124*(24), 13777–13802. https://doi.org/10.1029/2019JD030936

Shields, C. A., Kiehl, J. T., Rush, W., Rothstein, M., & Snyder, M. A. (2021). Atmospheric rivers in high-resolution simulations of the Paleocene Eocene Thermal Maximum (PETM). *Palaeogeography, Palaeoclimatology, Palaeoecology*, *567*, 110293. https://doi.org/10.1016/j.palaeo.2021.110293

Shields, C. A., Rosenbloom, N., Bates, S., Hannay, C., Hu, A., Payne, A. E., et al. (2019). Meridional heat transport during atmospheric rivers in high-resolution CESM climate projections. *Geophysical Research Letters*, *46*(24), 14702–14712. https://doi.org/10.1029/2019GL085565

Shields, C. A., Rutz, J. J., Leung, L. Y., Ralph, F. M., Wehner, M., Kawzenuk, B., et al. (2018). Atmospheric river tracking method intercomparison project (ARTMIP): Project goals and experimental design. *Geoscientific Model Development*, *11*(6), 2455–2474. https://doi.org/10.5194/gmd-11-2455-2018

Skinner, C. B., Lora, J. M., Payne, A. E., & Poulsen, C. J. (2020). Atmospheric river changes shaped mid-latitude hydroclimate since the mid-Holocene. *Earth and Planetary Science Letters*, *541*, 116293. https://doi.org/10.1016/j.epsl.2020.116293

Skinner, C. B., & Poulsen, C. J. (2016). The role of fall season tropical plumes in enhancing Saharan rainfall during the African Humid Period. *Geophysical Research Letters*, *43*(1), 349–358. https://doi.org/10.1002/2015GL066318

Smith, R. D., Jones, P., Briegleb, B., Bryan, F., Danabasoglu, G., Dennis, J., et al. (2010). *The parallel ocean program (POP) reference manual, ocean component of the community climate system model (CCSM), Tech. Rep. LAUR-10-01853* (p. 141). Los Alamos National Laboratory.

Spötl, C., Koltai, G., Jarosch, A. H., & Cheng, H. (2021). Increased autumn and winter precipitation during the Last Glacial Maximum in the European Alps. *Nature Communications*, *12*(1), 1839. https://doi.org/10.1038/s41467-021-22090-7

Tabor, C., Lofverstrom, M., Oster, J., Wortham, B., de Wet, C., Montañez, I., et al. (2021). A mechanistic understanding of oxygen isotopic changes in the western United States at the Last Glacial Maximum. *Quaternary Science Reviews*, *274*, 107255. https://doi.org/10.1016/j.quascirev.2021.107255

Wille, J. D., Favier, V., Dufour, A., Gorodetskaya, I. V., Turner, J., Agosta, C., & Codron, F. (2019). West Antarctic surface melt triggered by atmospheric rivers. *Nature Geoscience*, *12*(11), 911–916. https://doi.org/10.1038/s41561-019-0460-1

Wille, J. D., Favier, V., Gorodetskaya, I. V., Agosta, C., Kittel, C., Beeman, J. C., et al. (2021). Antarctic atmospheric river climatology and precipitation impacts. *Journal of Geophysical Research: Atmospheres*, *126*(8), e2020JD033788. https://doi.org/10.1029/2020JD033788

Wille, J. D., Favier, V., Jourdain, N. C., Kittel, C., Turton, J. V., Agosta, C., et al. (2022). Intense atmospheric rivers can weaken ice shelf stability at the Antarctic Peninsula. *Communications Earth & Environment*, *3*(1), 90. https://doi.org/10.1038/s43247-022-00422-9

Zhang, Z., Ralph, F. M., & Zheng, M. (2019). The relationship between extratropical cyclone strength and atmospheric river intensity and position. *Geophysical Research Letters*, *46*(3), 1814–1823. https://doi.org/10.1029/2018GL079071

Zhu, J., Otto-Bliesner, B. L., Brady, E. C., Poulsen, C. J., Tierney, J. E., Lofverstrom, M., & DiNezio, P. (2021). Assessment of equilibrium climate sensitivity of the Community Earth System Model version 2 through simulation of the Last Glacial Maximum. *Geophysical Research Letters*, *48*(3), e2020GL091220. https://doi.org/10.1029/2020GL091220

Zhu, Y., & Newell, R. E. (1998). A proposed algorithm for moisture fluxes from atmospheric rivers. *Monthly Weather Review*, *126*(3), 725–735. https://doi.org/10.1175/1520-0493(1998)126<0725:APAFMF>2.0.CO;2

Zwally, H. J., Abdalati, W., Herring, T., Larson, K., Saba, J., & Steffen, K. (2002). Surface melt-induced acceleration of Greenland Ice-Sheet flow. *Science*, *297*(5579), 218–222. https://doi.org/10.1126/science.1072708